

ANTHROPOGENIC REDUCTION OF SANTA ANA WINDS

A Paper From:
California Climate Change Center

Prepared By:
Mimi Hughes, Alex Hall, and Jinwon Kim

DISCLAIMER

This paper was prepared as the result of work sponsored by the California Energy Commission (Energy Commission) and the California Environmental Protection Agency (Cal/EPA). It does not necessarily represent the views of the Energy Commission, Cal/EPA, their employees, or the State of California. The Energy Commission, Cal/EPA, the State of California, their employees, contractors, and subcontractors make no warrant, express or implied, and assume no legal liability for the information in this paper; nor does any party represent that the uses of this information will not infringe upon privately owned rights. This paper has not been approved or disapproved by the California Energy Commission or Cal/EPA, nor has the California Energy Commission or Cal/EPA passed upon the accuracy or adequacy of the information in this paper.



Arnold Schwarzenegger, *Governor*

DRAFT PAPER

March 2009
CEC-500-2009-015-D

Acknowledgments

Mimi Hughes is supported by the University of California, Los Angeles, Dissertation Year Fellowship and National Science Foundation ATM-0735056, which also supports Alex Hall. Part of this work was performed using the National Center for Atmospheric Research supercomputer allocation 35681070. The research described in this paper was performed as an activity of the Joint Institute for Regional Earth System Science and Engineering, through an agreement between the University of California, Los Angeles, and the Jet Propulsion Laboratory, California Institute of Technology, and was sponsored by the National Aeronautics and Space Administration. Preprocessing of the Community Climate System Model data was also partially funded by the “National Comprehensive Measures against Climate Change” Program by Ministry of Environment, Korea (Grant No. 1700-1737-322-210-13) National Institute of Environmental Research, Korea. Computational resources for this study have been provided by Jet Propulsion Laboratory’s Supercomputing and Visualization Facility and the National Aeronautics and Space Administration’s Advanced Supercomputing Division.

Preface

The California Energy Commission's Public Interest Energy Research (PIER) Program supports public interest energy research and development that will help improve the quality of life in California by bringing environmentally safe, affordable, and reliable energy services and products to the marketplace.

The PIER Program conducts public interest research, development, and demonstration (RD&D) projects to benefit California's electricity and natural gas ratepayers. The PIER Program strives to conduct the most promising public interest energy research by partnering with RD&D entities, including individuals, businesses, utilities, and public or private research institutions.

PIER funding efforts focus on the following RD&D program areas:

- Buildings End-Use Energy Efficiency
- Energy-Related Environmental Research
- Energy Systems Integration
- Environmentally Preferred Advanced Generation
- Industrial/ Agricultural/ Water End-Use Energy Efficiency
- Renewable Energy Technologies
- Transportation

In 2003, the California Energy Commission's PIER Program established the **California Climate Change Center** to document climate change research relevant to the states. This center is a virtual organization with core research activities at Scripps Institution of Oceanography and the University of California, Berkeley, complemented by efforts at other research institutions. Priority research areas defined in PIER's five-year Climate Change Research Plan are: monitoring, analysis, and modeling of climate; analysis of options to reduce greenhouse gas emissions; assessment of physical impacts and of adaptation strategies; and analysis of the economic consequences of both climate change impacts and the efforts designed to reduce emissions.

The California Climate Change Center Report Series details ongoing center-sponsored research. As interim project results, the information contained in these reports may change; authors should be contacted for the most recent project results. By providing ready access to this timely research, the center seeks to inform the public and expand dissemination of climate change information, thereby leveraging collaborative efforts and increasing the benefits of this research to California's citizens, environment, and economy.

For more information on the PIER Program, please visit the Energy Commission's website www.energy.ca.gov/pier/ or contract the Energy Commission at (916) 654-5164.

Table of Contents

| | |
|--|-----|
| Preface..... | iii |
| Abstract..... | vii |
| 1.0 Introduction..... | 1 |
| 2.0 Data..... | 2 |
| 2.1. MM5 Simulation..... | 2 |
| 2.2. Weather Research and Forecast (WRF) Simulation..... | 4 |
| 3.0 A Santa Ana Index..... | 4 |
| 4.0 Santa Ana Response to a Changing Climate..... | 5 |
| 5.0 Understanding Reduced Santa Ana Frequency..... | 7 |
| 6.0 Conclusions..... | 15 |
| 7.0 References..... | 16 |

List of Figures

Figure 1. Correlation of observed offshore component of wintertime daily winds with that from the MM5 simulation at the nearest gridpoint. This downscaling uses Eta model analysis data available through the National Center for Atmospheric Research’s GEWEX Continental Scale International Project (GCIP) archive for its initial and lateral boundary conditions and covers the time period 1995 through 2006. Black contours show model terrain, plotted every 800 m starting at 100 m. Thick black contour shows coastline at 6 km resolution.....3

Figure 2. Average winds for days with Santa Ana time series greater than 8 m s^{-1} for (a) MM5 simulation and (b) WRF present day simulation. Arrows show total wind; color contours show wind speed. Only every third grid point is plotted for clarity. Black contours show model terrain, plotted every 800 meters (m) starting at 100 m. The thick black contour in panel (a) shows coastline at 6-km resolution, and in panel (b) at 12-km resolution. Panel (c) shows the magnitude of the Santa Ana time index (SAI) for entire 44-year time period. The thin dashed black line shows $\text{SAI} = 8 \text{ m s}^{-1}$, the threshold used to define a Santa Ana in panels (a) and (b) and for the red line of Figure 3.6

Figure 3. Total number of days for each winter season where SAI is greater than 6, 8, or 10 m s^{-1} (blue, red, and green line, respectively) in the MM5 simulation. Dashed lines show linear trend. The winter season is defined as October to March, and the year label is the year in which the season begins (e.g., 1959 is Oct. 1959 to Apr. 1960). Inset: Number of days per

season with SAt greater than 10 m s^{-1} in the WRF (green bar) present day and (yellow bar) future simulation. All trends are significant at the 99% confidence level using a two-tailed t-test.7

Figure 4. Santa Ana time index versus (a) 700 hPa mean geopotential height anomaly and (b) buoyancy-induced pressure gradient force, for winter days when the wind 2 kilometers above sea level in the Mojave desert has an offshore component. The points are color coded by the magnitude of the offshore component of the desert wind 2 kilometers above sea level for each point (reference colorbar is at bottom). Data is the MM5 downscaling with Eta model analysis as boundary conditions, as in Figure 1. 10

Figure 5. Actual SAt plotted against that predicted by the bivariate regression model (\hat{SAt}) for (a) MM5 simulation, 1959–1969, (b) MM5 simulation, 1991–2001, (c) WRF present-day simulation, and (d) WRF future climate simulation. Red dashed line shows $SAt = \hat{SAt}$ 11

Figure 6. Total contribution of (left grouping) β and (right grouping) u to SAt for (a) MM5 simulation and (b) WRF simulation. Contributions were calculated by summing the product of the regression model parameters and (left column) β or (right column) u for days with SAt greater than (a) 8 m s^{-1} and (b) 14 m s^{-1} 13

Figure 7. Seasonal mean sea level pressure (SLP) anomaly in the Great Basin (40N, 110W), from the ERA-40 data. Black dashed line shows linear trend. (Inset) Mean surface pressure in the Great Basin in the 36-km WRF downscaling of the CCSM data for the present-day (green bar) and future scenarios (yellow bar). Trend is significant at the 90% confidence level using a one-tailed t-test. 14

Figure 8. Seasonal mean temperature at the desert surface (blue line) and air temperature 1.2 km above the ocean surface. Dashed lines show linear trend. (Inset) Change in mean temperature between the present and future WRF simulations at the desert surface (blue bar) and 1.2 km over the ocean surface (red bar). Trend in desert surface air temperature is significant at the 90% confidence level using a one-tailed t-test; trend in air temperature over the ocean is not significant. 15

List of Tables

Table 1. Coefficients of the bivariate regression model (Eq. 1). Units are shown in the header row. 12

Abstract

The frequency of Santa Ana wind events is investigated within a high-resolution downscaling of the European Centre for Medium-Range Weather Forecasts ERA-40 reanalysis data to 6-kilometer resolution over Southern California. In this climate reconstruction, the number of Santa Ana days per winter season declines significantly over the 44-year reanalysis period, resulting in over 30 percent fewer events per year over the final decade of the reconstruction (1991–2001) compared to the first decade (1959–1969). This study investigates this signal further in late-twentieth and mid-twenty-first century realizations of the National Center for Atmospheric Research Community Climate System Model, version 3.0, global climate change scenario run downscaled to a 12-kilometer resolution over California. The reduction in events per year in the mid-twenty-first century compared with the late-twentieth century is similar to that seen in the ERA-40 downscaling, suggesting the cause of the decrease is a change in the climate due to anthropogenic forcing. A regression model is used to reproduce the Santa Ana time series based on two previously documented forcing mechanisms: synoptically-forced strong offshore winds at the mountain tops (which transport offshore momentum to the surface), and a local desert-ocean temperature gradient causing katabatic-like winds as the cold desert air pours down the coastal topography. Both past and future climate simulations show a large reduction in the contribution of the local thermodynamic forcing. This reduction is due to the differential warming that occurs during transient climate change conditions, with more warming in the desert interior than over the ocean. Thus the mechanism responsible for the decrease in Santa Ana frequency originates from a well-known aspect of the climate response to increasing greenhouse gases, but cannot be understood or simulated without mesoscale atmospheric dynamics.

Keywords: Regional climate, climate change, Santa Ana winds, fire weather, Southern California

1.0 Introduction

The cool, moist fall and winter climate of Southern California is often disrupted by dry, hot days with strong winds, known as Santa Anas, blowing out of the desert. The Santa Ana winds are a dominant feature of the fall and wintertime climate of Southern California (Conil and Hall 2006), and they have important ecological impacts. First, and most pronounced, is their influence on wildfires: following the hot, dry Southern California summer, the extremely low relative humidities and gusty strong winds that occur during Santa Anas introduce extreme fire risk which often culminates in wildfires with large economic loss (Westerling et al. 2004). Less familiar but just as important is their impact on coastal-ocean ecosystems: The strong winds induce cold filaments in sea-surface temperature (SST) with an associated increase in biological activity (Castro et al. 2006; Trasvina et al. 2003). This decrease in SST and increase in biological activity is likely due in part to increased mixing in the oceanic boundary layer, although an increase in dust deposition on the ocean surface during these events could also increase biological activity (Hu and Liu 2003; Jickells et al. 2005).

Despite their importance to local climate, very few studies examine their variability on timescales longer than a few months (Finley and Raphael 2007; Raphael 2003; Schroeder et al. 1964; Edinger et al. 1964). Furthermore, all but the oldest of these studies rely on a large-scale proxy for the local Santa Ana wind intensity, which may not be representative of actual changes to their frequency (Hughes and Hall 2009). In a recent study, Miller and Schlegel (2006) documented how Santa Ana wind frequency may change under anthropogenic climate change conditions; however, similar to the above-mentioned studies, they use a large-scale proxy to indicate their occurrence.

This study investigates the response of the frequency and intensity of Santa Ana events to anthropogenic climate change. Unlike previous studies, we identify Santa Ana wind events by the strength of the offshore wind through the gaps in Southern California's topography. To accomplish this local perspective, we downscale the European Centre for Medium-Range Weather Forecasts (ECMWF) reanalysis data and a coarse-resolution climate model with regional atmospheric models. This dynamical downscaling technique has been proven numerous times to give a more realistic view of local climate conditions (e.g., Diffenbaugh et al. 2005; Leung and Ghan 1999), and when utilized with reanalysis products, provide a reasonably accurate representation of a region's climate (Conil and Hall 2006; Hughes and Hall 2008; Hughes et al. 2008; Kanamitsu and Kanamaru 2007a,b). Our results indicate that as the climate begins to adjust to increased greenhouse gas forcing, the frequency of Santa Ana days is reduced.

A recent investigation of the dynamics of Santa Ana winds (Hughes and Hall 2009) found that both local and synoptic conditions control their formation. Similar to the results of Gabersek and Durran (2006), when strong synoptically forced offshore flow impinges on Southern California's topography, offshore momentum can be transported to the surface, causing Santa Ana conditions. However, Hughes and Hall (2009) found that there are many days with Santa Ana conditions that are not associated with this type of strong synoptic forcing. Rather, for a large fraction of the Santa Ana days, offshore winds are forced by a local temperature gradient between the cold desert and warmer air over the ocean at the same altitude. The temperature gradient induces a hydrostatic pressure gradient pointing from the desert to the ocean, which is

reinforced by the negative buoyancy of the cold air as it flows down the sloped surface of the major topographical gaps. This mechanism is essentially the same the one driving katabatic winds of Antarctica (Parish and Cassano 2003; Barry 1992). Often both mechanisms are at play, because the synoptic conditions causing strong offshore flow aloft—a high-pressure system over the northwestern U.S. coast—also favor cold advection into the desert. This is most often the case during the strongest Santa Ana days. As we demonstrate, this understanding of the dynamics of Santa Ana winds allows us to identify how large-scale changes in the future climate affect the frequency and intensity of Santa Ana events.

2.0 Data

Santa Ana wind event history over the last half-century is identified using a dynamical downscaling of atmospheric reanalysis, described in Section 2.1. The climate change experiment is carried out by downscaling a “present-day” and “future” Community Climate System Model, version 3 (CCSM3) simulation, as described in Section 2.2. Although the simulations are achieved using two different regional models—the Penn State/National Center for Atmospheric Research (NCAR) mesoscale model version 5 (MM5) and the Weather Research and Forecast (WRF) model—the two products are utilized separately, with the MM5 downscaling providing conditions during the observational period and the WRF simulation quantifying the anthropogenic climate change signal.

The carbon dioxide (CO₂) concentrations in the WRF simulations were fixed at 330 parts per million, volume (ppmv) and 430 ppmv during the present-day and mid-twenty-first century periods, respectively; whereas the greenhouse gas concentrations in the MM5 downscaling are fixed for the 44-year simulation. However, increasing greenhouse gases in a regional model has almost no effect on the climate unless the larger-scale boundary conditions also change. Thus the differences between the two WRF simulations are due to the different boundary conditions (i.e., the large-scale response to increased greenhouse gases) and not to the greenhouse gas increase in WRF itself. Further, the MM5 downscaling contains information about the changing climate because of its reanalysis boundary conditions.

2.1. MM5 Simulation

Identification of events in the actual climate and weather conditions of the last half-century is given by a high-resolution simulation created with the mesoscale model version 5 (MM5), release 3.6.0 (Grell et al. 1994). The 6-kilometer (km) domain was nested within an 18-km domain covering Southern California and parts of Arizona, Nevada, and Mexico, which was likewise nested within a 54-km domain encompassing most of the western United States. At this resolution, all major mountain complexes in Southern California are represented, as are the Channel Islands just off the coast. The number of gridpoints in each domain are 35 × 36, 37 × 52, and 55 × 97 for the 54-, 18-, and 6-km domains, respectively, and the nesting was two-way for both interior domains. Each domain has 23 vertical levels, with the vertical grid stretched to place the highest resolution in the lower troposphere. In the outer two domains, the Kain-Fritsch 2 (Kain 2002) cumulus parameterization scheme was used. In the 6-km domain, only explicitly resolved convection could occur. In all domains, we used the Medium Range Forecast (MRF) boundary layer scheme (Hong and Pan 1996), Dudhia simple ice microphysics (Dudhia 1989), and a radiation scheme simulating longwave and shortwave interactions with clear-air and cloud (Dudhia 1989).

The atmospheric boundary conditions for the simulation come from ECMWF’s 45-year reanalysis data (ERA-40, Uppala et al. 2005) available through NCAR’s Computational and Information Systems Laboratory. The sea-surface temperature (SST) comes from the Smith and Reynolds Extended Reconstructed SST dataset for 1959–1980 (Smith and Reynolds 2003) and the National Oceanic and Atmospheric Administration (NOAA) Optimum Interpolation Sea Surface Temperature Analysis after 1981 (Reynolds et al. 2002); the SST data was linearly interpolated in time to six-hour intervals. The time period covered in the simulation was from January 1959 to August 2002. Throughout this period, MM5 was initialized every 15 days at 18Z (10 a.m. local time) and run for 366 hours, with the first six hours being discarded as model spin-up. The interior boundary conditions were updated at each initialization, with the sea-surface temperatures and lateral boundary conditions updated continuously throughout the run. Thus the simulation in the 6-km nest acts as a reconstruction of the local atmospheric conditions based on known large-scale atmospheric conditions.

We confirm the effectiveness of this downscaling technique in reconstructing local circulation anomalies by showing the correlation of the observed offshore component of the wind (i.e., the component most aligned with the Santa Anas) with MM5 winds at the nearest gridpoint for days where the winds 2 kilometers above sea level in the desert have an offshore component (Figure 1). The correlations are larger than 0.4 in all but five of the 42 locations, and larger than 0.7 at 13 locations, many of which are near the largest gaps in the topography. This high degree of correspondence with observations gives us a reasonable degree of confidence in the simulation’s fidelity.

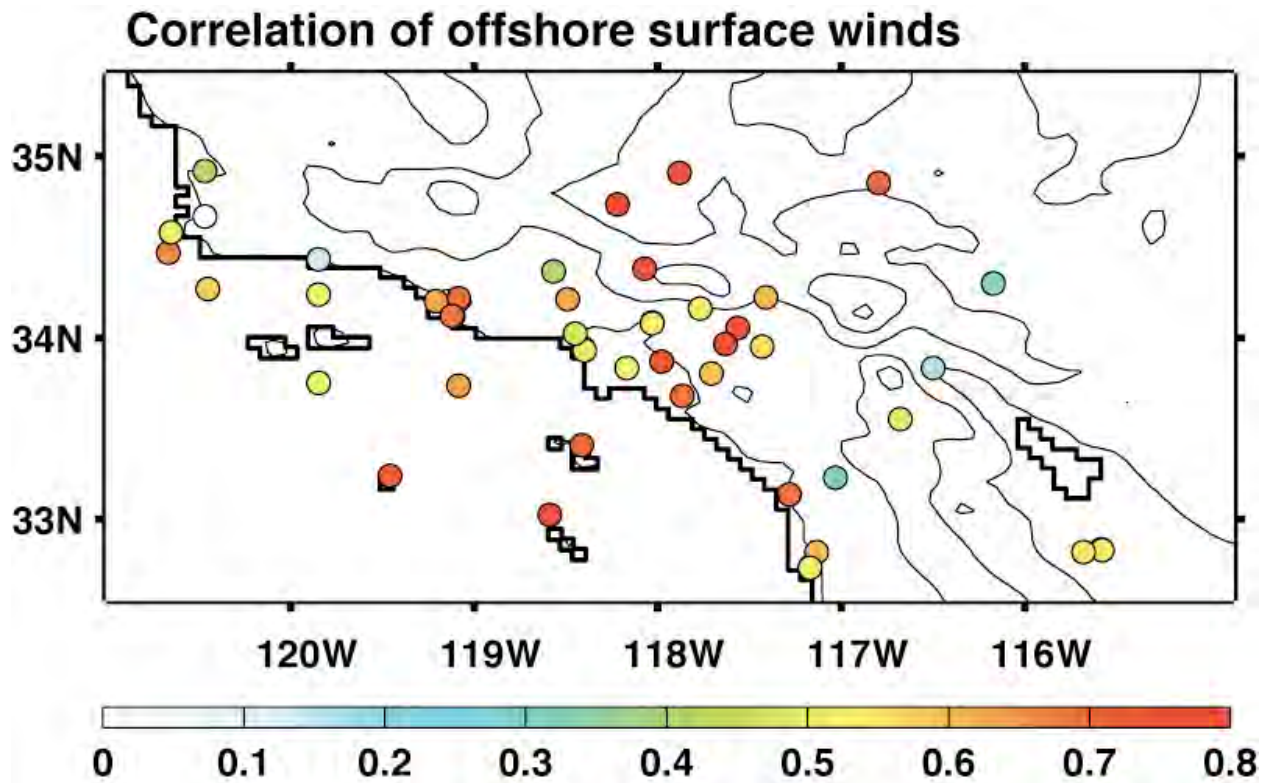


Figure 1. Correlation of observed offshore component of wintertime daily winds with that from the MM5 simulation at the nearest gridpoint. This downscaling uses Eta model analysis data available through the National Center for Atmospheric Research’s GEWEX Continental Scale

International Project (GCIP) archive for its initial and lateral boundary conditions and covers the time period 1995 through 2006. Black contours show model terrain, plotted every 800 m starting at 100 m. Thick black contour shows coastline at 6 km resolution.

2.2. Weather Research and Forecast (WRF) Simulation

The dynamical downscaling for the climate change scenario was performed using the Weather Research and Forecast (WRF) model, version 2.2.1 (Skamarock et al. 2005). Similar to MM5, the model solves a non-hydrostatic momentum equation in conjunction with the thermodynamic energy equation. The model features multiple options for advection and the parameterized atmospheric physical processes. The physics options selected in this experiment include the NOAA¹ land-surface scheme (Chang et al. 1999), the simplified Arakawa Schubert (SAS) convection scheme (Hong and Pan 1998), the Rapid Radiative Transfer Model (RRTM) longwave radiation scheme (Mlawer et al. 1997), Dudhia (1989) shortwave radiation, and the WRF Single-Moment (WSM) 3-class with simple ice cloud microphysics scheme. For more details on the physics options, readers are referred to the website <http://wrf-model.org>. The model domain covers the western United States at a 36-km horizontal resolution, with the inner 12-km nest spanning the entire coast of California. Both domains have 28 atmospheric and 4 soil layers in the vertical.

The regional climate simulations were driven by the global climate data generated by the NCAR CCSM3 when the *Special Report on Emissions Scenarios* (SRES) A1B emission scenario is imposed (Nakicenovic and Swart 2000). The emission scenario assumes balanced energy generation between fossil and non-fossil fuel; the resulting carbon dioxide (CO₂) emissions are located near the averages of all SRES emission scenarios. The climatology for the late twentieth century and mid-twenty-first century periods is calculated from the 10 cold season (October–March) regional simulations for 1971–1981 and 2045–2055, respectively. Individual runs were initialized at 00UTC October 1 of the corresponding years using the CCSM-3 output data. All simulations continued for the remaining six-month period without re-initialization by updating the large-scale forcing along the lateral boundaries at three-hour intervals.

3.0 A Santa Ana Index

The first step in identifying the local and synoptic scale atmospheric conditions associated with Santa Ana (SA) winds is to create a SA index. In the past, this has been done in numerous ways. Two recent studies have used large-scale surface pressure conditions, a high over the Great Basin and a low southwest of Los Angeles, to identify Santa Ana events (Miller and Schlegel 2006; Raphael 2003). Operational definitions combine this pressure gradient with two other parameters, the relative humidity in coastal Southern California and wind direction in major mountain passes (Sommers 1978; D. Danielson 2007, personal communication). Conil and Hall (2006) used a mixture model cluster analysis of the daily mean wind anomalies to classify the winter circulation into three regimes, one of which was Santa Ana events.

¹ The acronym stems from N: National Centers for Environmental Prediction (NCEP); O: Oregon State University (Dept of Atmospheric Sciences); A: Air Force (both AFWA and AFRL); and H: Hydrologic Research Lab - NWS (now Office of Hydrologic Development, or OHD).

For this study, we seek a SA index that does not introduce assumptions about large-scale mechanisms possibly causing Santa Anas. The operational and large-scale definitions do not meet this criterion. Further, we also seek an index that gives information about SA intensity. However, the cluster model classification technique gives no indication about the strength of the offshore flow and rather simply classifies a day as experiencing Santa Ana conditions or not. Since no previous metric meets our needs, we develop a new SA index based on the magnitude of a spatially extensive offshore wind in the local circulation.

We create a SA index that is simply the offshore wind strength at the exit of the largest gap (blue box, Figure 2a and b); the resulting time index, SA_t , is shown for the MM5 simulation in Figure 2c. To illustrate that this index agrees with previous measures of SA intensity, Figure 2a and 2b show the composite surface winds for days with SA_t greater than 8 meters per second ($m\ s^{-1}$) for subsets of the MM5 and WRF simulations, respectively. The composite SA wind fields exhibit characteristics we expect for SA events: strong offshore (that is, roughly northeasterly) winds throughout most of Southern California, with the strongest winds on the leeward slopes of the mountains and through the gaps in the topography, most notably across the Santa Monica mountains.

Our index has a very strong seasonality (Figure 2c), with peak occurrence in December and no strong offshore winds from April to September. This agrees with previous indices of SA occurrence (Hughes and Hall 2009; Conil and Hall 2006; Raphael 2003). Because of this strong seasonality, from here on we only consider days between October and March and refer to them as “winter” days.

4.0 Santa Ana Response to a Changing Climate

Is there any change in the number of SA days due to anthropogenic forcing? To answer this question, we first examine the frequency of SA wind events in the 44-year MM5 simulation. Figure 3 shows the total number of winter days that have SA_t greater than 6, 8, and 10 $m\ s^{-1}$ (blue, red, and green lines). We show the results for 6 and 10 $m\ s^{-1}$ to illustrate that the results are not sensitive to the threshold chosen as representing a SA day. There is a substantial decrease in the number of SA days per winter season as we move from the 1960s to the current century, with the 1990s experiencing nearly 1/3 as many SA days as the 1960s.

This dramatic reduction in SA events over the last half of the twentieth century suggests that increasing greenhouse gases and the associated climatic response could cause a change in SA frequency. To test whether this change is indeed anthropogenic in origin, we now turn our attention to SA days in the WRF downscaling of CCSM. To the extent that there is a difference between the two WRF simulations, we know it is due to the effect of increased greenhouse gases in the CCSM boundary conditions, since that is the only difference between the two simulations. The inset panel of Figure 3 shows the average number of days with SA_t greater than 10 $m\ s^{-1}$ for the late-twentieth and mid-twenty-first century WRF simulations; we use a larger threshold to define a SA day in the WRF simulations because the WRF simulation has a slight climatological bias towards stronger offshore winds, but the results are relatively insensitive to this threshold. There is nearly a 20% reduction in the total number of SA days per year in the mid-twenty-first century run.

Because the CCSM-forced WRF simulation shows a qualitatively similar reduction in SA wind occurrence to the MM5 run, the reduction in the MM5 downscaling is probably also due to changes in the climate from anthropogenic forcing. In the following sections, we explore the mechanism by which the frequency of SA wind events is reduced to lend more credibility to this result.

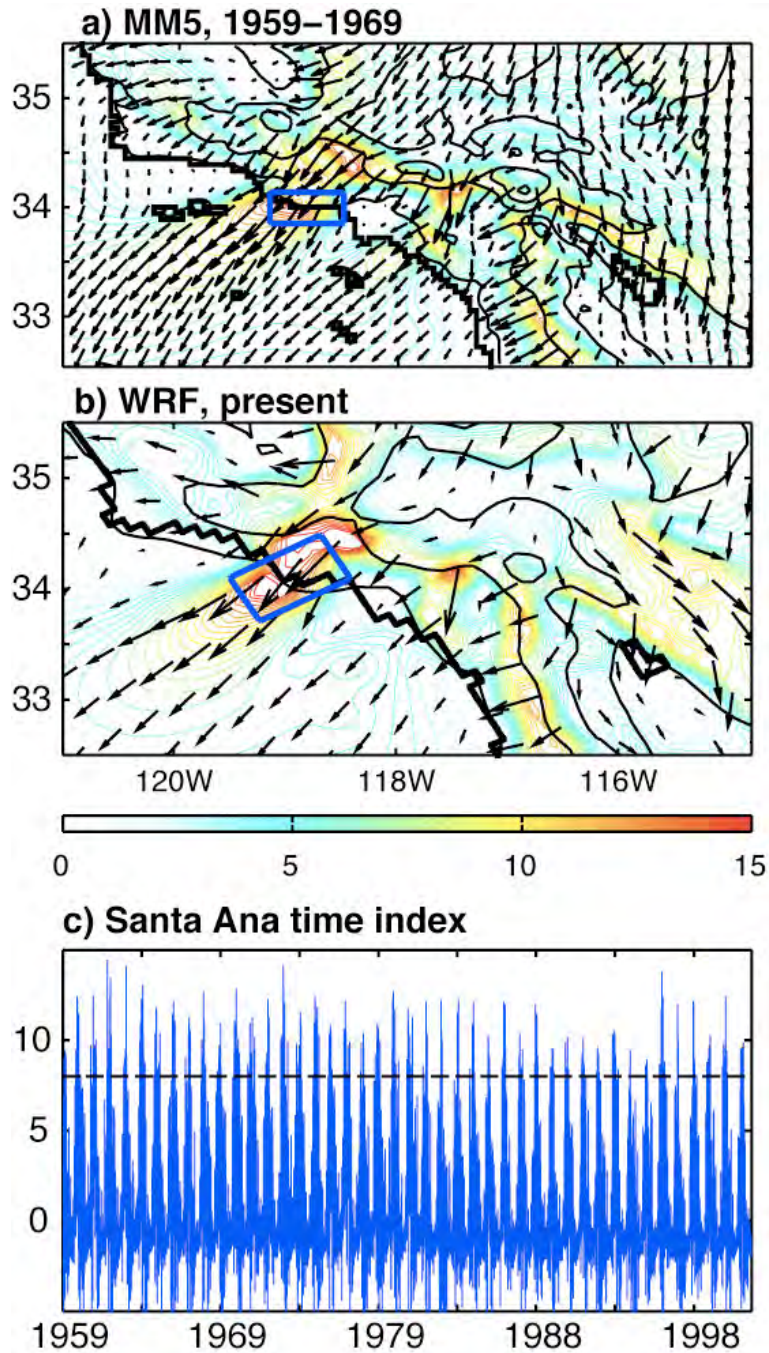


Figure 2. Average winds for days with Santa Ana time series greater than 8 m s^{-1} for (a) MM5 simulation and (b) WRF present

day simulation. Arrows show total wind; color contours show wind speed. Only every third grid point is plotted for clarity. Black contours show model terrain, plotted every 800 meters (m) starting at 100 m. The thick black contour in panel (a) shows coastline at 6-km resolution, and in panel (b) at 12-km resolution. Panel (c) shows the magnitude of the Santa Ana time index (SA_t) for entire 44-year time period. The thin dashed black line shows SA_t = 8 m s⁻¹, the threshold used to define a Santa Ana in panels (a) and (b) and for the red line of Figure 3.

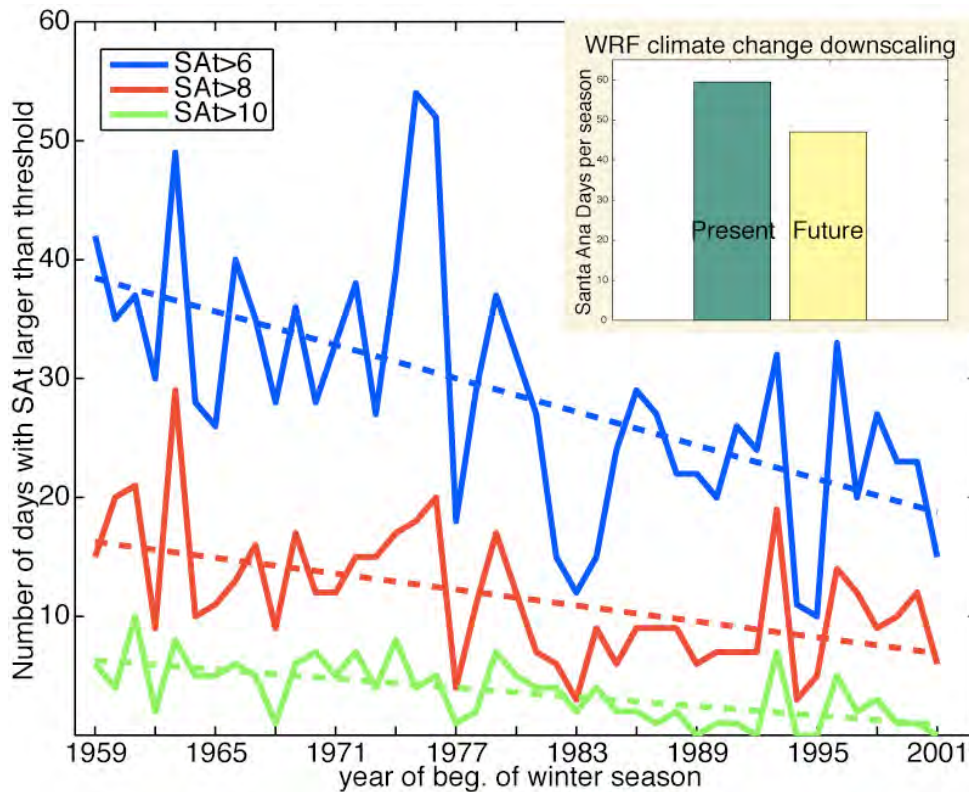


Figure 3. Total number of days for each winter season where SA_t is greater than 6, 8, or 10 m s⁻¹ (blue, red, and green line, respectively) in the MM5 simulation. Dashed lines show linear trend. The winter season is defined as October to March, and the year label is the year in which the season begins (e.g., 1959 is Oct. 1959 to Apr. 1960). Inset: Number of days per season with SA_t greater than 10 m s⁻¹ in the WRF (green bar) present day and (yellow bar) future simulation. All trends are significant at the 99% confidence level using a two-tailed t-test.

5.0 Understanding Reduced Santa Ana Frequency

The dynamics controlling the formation of SA winds were recently investigated by Hughes and Hall (2009). They found that SAs arise from a combination of two mechanisms—synoptic and local thermodynamically driven. Here we reproduce important results to clarify the reason for reduced SA frequency.

Previous studies identified large-scale mid-tropospheric conditions as the driver of SAs (e.g., Sommers 1978). If there is a large synoptic-scale pressure gradient causing strong offshore winds over Southern California at mountain-top level, this causes strong surface flow as the offshore momentum is transferred to the surface in a vertically stably stratified atmosphere. This often occurs when a high surface pressure anomaly is located over the Great Basin, with a corresponding high geopotential height anomaly at 700 hectopascals (hPa) centered over the Oregon coast. In fact, this is exactly the pattern that appears if composite maps are made for the synoptic conditions during SA days (not shown). An examination of the relationship between this geopotential height (GPH) anomaly at 700 hPa and SAT (Figure 4a) reveals a tendency for large SAT when a large GPH anomaly exists. However, this relationship only modestly explains the variability in SAT (correlation coefficient = 0.56): there are many days with large SAT and weak synoptic forcing and conversely many days with large synoptic forcing and small SAT.

Since synoptic forcing only explains a small amount of the variability in SAT, Hughes and Hall (2009) sought another mechanism controlling SA formation. They found that if a large temperature gradient exists between the cold desert surface and the warm ocean air at the same altitude (approximately 1.2 km), it causes a localized offshore pressure gradient near the surface. This in turn generates katabatic-like offshore flow in a thin layer near the surface, as the negatively buoyant, cold desert air flows down the sloped surface of the gaps. The negative buoyancy can be written as a pressure gradient force (Parish and Cassano 2003):

$$\beta = \frac{g\theta'}{\theta_0} \sin(\alpha), \quad (\text{Eq. 1})$$

where $g=9.8 \text{ ms}^{-1}$ is gravitational acceleration, θ' is the temperature deficit of the cold layer, θ_0 is the average temperature in the cold layer, and α is the slope of the topography. To calculate β , we use the average desert surface temperature for θ_0 , the average slope of the topography through the largest gap for α (approximately 1 degree, or 1 km drop over 50 km; see Figure 2a) and the temperature difference between the cold desert surface (i.e., the cold layer) and air over the ocean at the same altitude (representative of the ambient atmosphere) for θ' . The relationship between β and SAT is strong and linear (Figure 4b), with a much higher correlation (correlation coefficient = 0.88) than was found between SAT and GPH anomaly, suggesting β strongly influences SAT variability.

These two mechanisms can act independently, causing mild SA winds, or combine to force the largest magnitude offshore winds. This joint contribution to SAT is captured by a bivariate regression model to predict SAT based on two parameters representative of each mechanism (Hughes and Hall 2009):

$$\hat{SAT}(u, \beta) = A * u + B * \beta + C, \quad (\text{Eq. 2})$$

where u , the offshore wind speed at 2 km, represents the synoptic forcing and β represents the local thermodynamic forcing.

Figure 5 shows the regression model's representation of SAT, \hat{SAT} , plotted against SAT for the first and last decade of the MM5 downscaling (Figure 5a and b) and the WRF downscaling simulations (Figure 5c and d). The high degree of correspondence (correlation coefficient = 0.91, 0.91, 0.88, and 0.86 for the two MM5 time periods and WRF present and future simulations, respectively) confirms that the two mechanisms are primarily responsible for determining SAT in all simulations. The coefficients of the model are similar within the two MM5 time periods and the two WRF simulations (Table 1), but they do vary somewhat between the regional models. In particular, the WRF simulations display larger sensitivity to variations in β (e.g., $B=983 \text{ s}^{-1}$ for MM5 1959–1969 and $B=2443 \text{ s}^{-1}$ for WRF present); this may partially explain the tendency for larger SAT in those simulations.

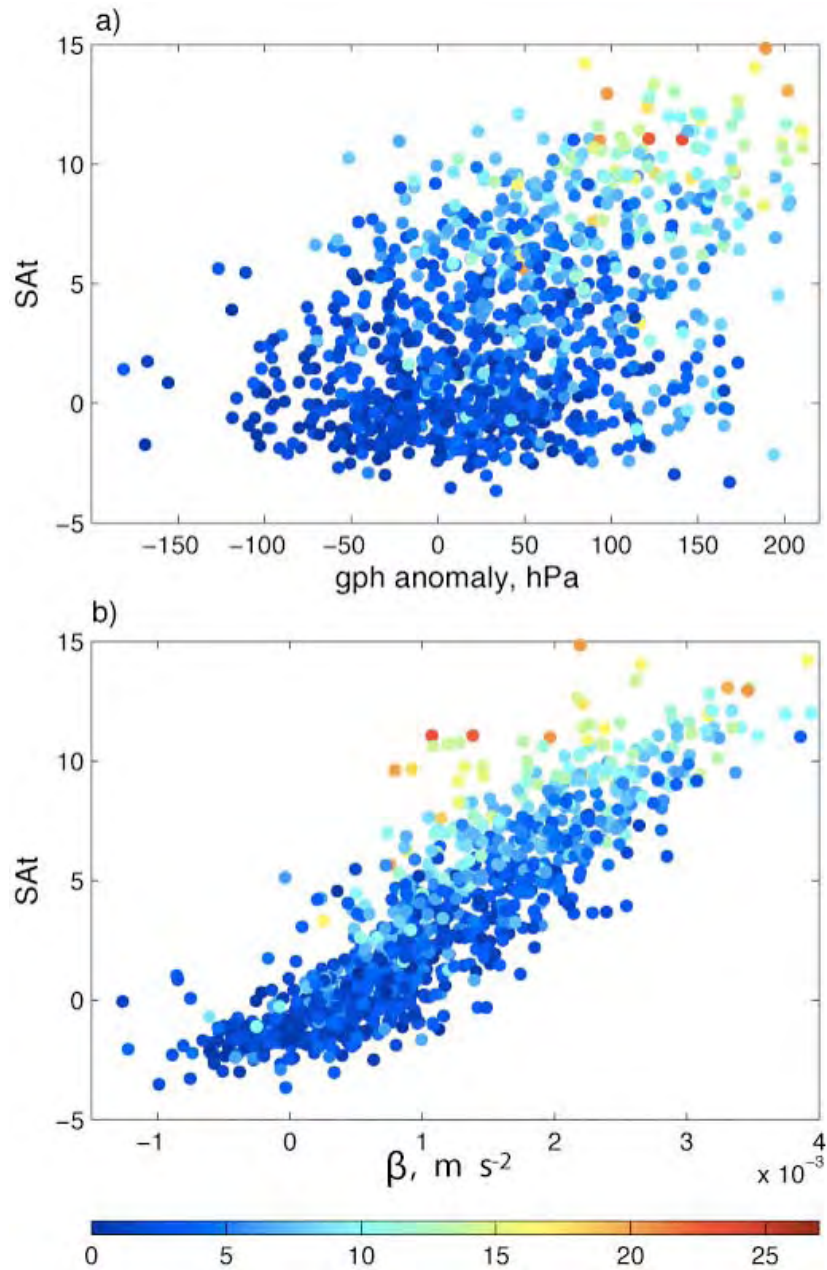


Figure 4. Santa Ana time index versus (a) 700 hPa mean geopotential height anomaly and (b) buoyancy-induced pressure gradient force, for winter days when the wind 2 kilometers above sea level in the Mojave desert has an offshore component. The points are color coded by the magnitude of the offshore component of the desert wind 2 kilometers above sea level for each point (reference colorbar is at bottom). Data is the MM5 downscaling with Eta model analysis as boundary conditions, as in Figure 1.

Because it represents distinct physical processes, the regression model allows us to identify the changes in forcing responsible for the reduction in SAT in both the observed time series and the WRF climate change simulations. To understand which term of the regression model is causing reduced \widehat{SAT} , we calculate the total contribution of β and u to \widehat{SAT} separately and then sum over days with \widehat{SAT} greater than 8 m s^{-1} (14 m s^{-1}) for the MM5 (WRF) time periods (Figure 6).

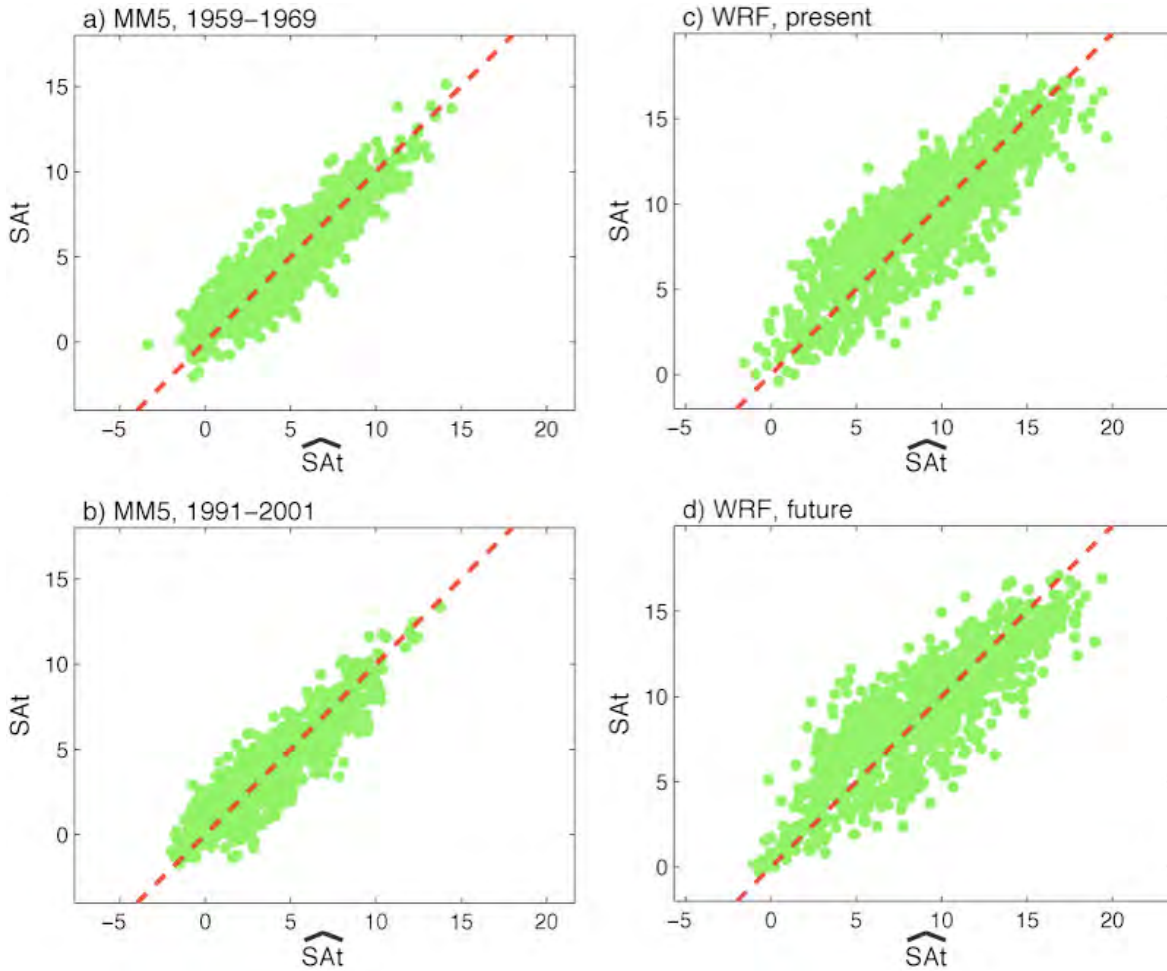


Figure 5. Actual SAT plotted against that predicted by the bivariate regression model (\widehat{SAT}) for (a) MM5 simulation, 1959–1969, (b) MM5 simulation, 1991–2001, (c) WRF present-day simulation, and (d) WRF future climate simulation. Red dashed line shows $SAT = \widehat{SAT}$.

Table 1. Coefficients of the bivariate regression model (Eq. 1). Units are shown in the header row.

| | A (dimensionless) | B (s⁻¹) | C (m s⁻¹) |
|----------------------|--------------------------|---------------------------|-----------------------------|
| MM5 1959–1969 | 0.41 | 983 | 0.70 |
| MM5 1991–2001 | 0.42 | 953 | 0.11 |
| WRF Present | 0.36 | 2443 | 0.15 |
| WRF Future | 0.33 | 2704 | 0.08 |

Turning our attention first to the synoptic forcing represented by u in Eq. 1 and the second column grouping in Figure 6, we see that the MM5 simulation shows a large reduction in contribution of synoptic forcing from the 1960s to the 1990s while the WRF simulation shows almost no change between the present and future simulations. Because the synoptic activity often associated with SA events often involves a high pressure system centered over the Great Basin at the surface (e.g., Hughes and Hall 2009; Conil and Hall 2006; Raphael 2003), we examine the seasonal mean sea-level pressure (SLP) anomaly in the Great Basin with the assumption that this is representative of the synoptic variability on shorter time scales. The Great Basin SLP anomaly in ERA-40 shows a statistically significant negative trend over the last half century (Figure 7), consistent with the reduced synoptic forcing of SA winds seen in the MM5 downscaling. However, this reduction is absent in the WRF downscaling suggesting that this reduced synoptic forcing is either not anthropogenically forced or is caused by a response to increased greenhouse gases not captured by the CCSM simulations.

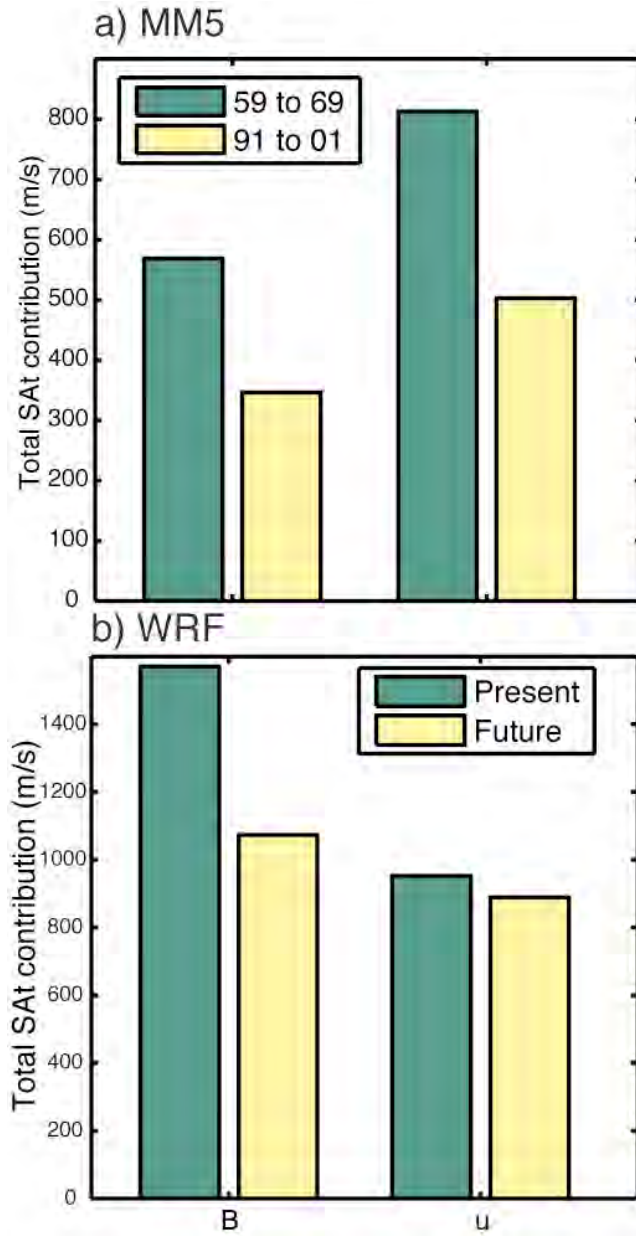


Figure 6. Total contribution of (left grouping) β and (right grouping) u to SAT for (a) MM5 simulation and (b) WRF simulation. Contributions were calculated by summing the product of the regression model parameters and (left column) β or (right column) u for days with SAT greater than (a) 8 m s^{-1} and (b) 14 m s^{-1} .

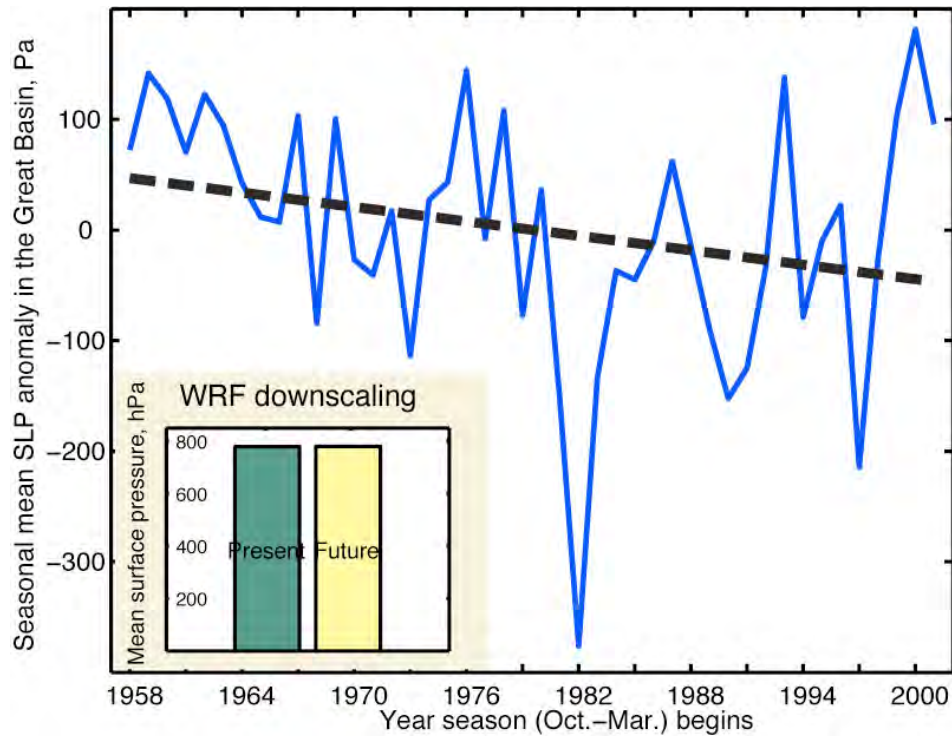


Figure 7. Seasonal mean sea level pressure (SLP) anomaly in the Great Basin (40N, 110W), from the ERA-40 data. Black dashed line shows linear trend. (Inset) Mean surface pressure in the Great Basin in the 36-km WRF downscaling of the CCSM data for the present-day (green bar) and future scenarios (yellow bar). Trend is significant at the 90% confidence level using a one-tailed t-test.

Focusing instead on the katabatic forcing of β in Eq. 1 and the first column grouping in Figure 6, we see that both simulations show over 1/3 less contribution to $\hat{S}\hat{A}t$ from β as the climate responds to increased greenhouse gas forcing. This is because land masses respond more quickly to increased radiative forcing than the oceans (e.g. Trenberth et al. 2007). Figure 8 shows the seasonal mean desert surface air temperature (SAT) as well as the air temperature over the ocean at the same altitude—the two components of θ' used to calculate β —from the MM5 simulation (main panel). Both temperatures show a positive trend over the 44-year time series, but the desert surface air temperature increases more than the ocean temperature (note that the trend of the air over the ocean is not significantly different from zero). The magnitude of the katabatic pressure gradient, β , is directly proportional to the difference between these two temperatures. So as the desert warms faster than the air over the ocean, a large temperature gradient between the two areas becomes less likely in wintertime, and large β becomes less frequent. Examining the corresponding change in the WRF simulation (Figure 8, inset), we see that the desert SAT warms about a degree more than the air over the ocean at the same altitude, similar to the observed trend although larger in magnitude. Because the only difference between the two periods of the CCSM simulation is the increase in greenhouse gas forcing, this decrease in the desert-ocean temperature gradient must be anthropogenically forced. It follows that the reduction in β and the resulting decrease in SA frequency also arises from the increase in greenhouse gases.

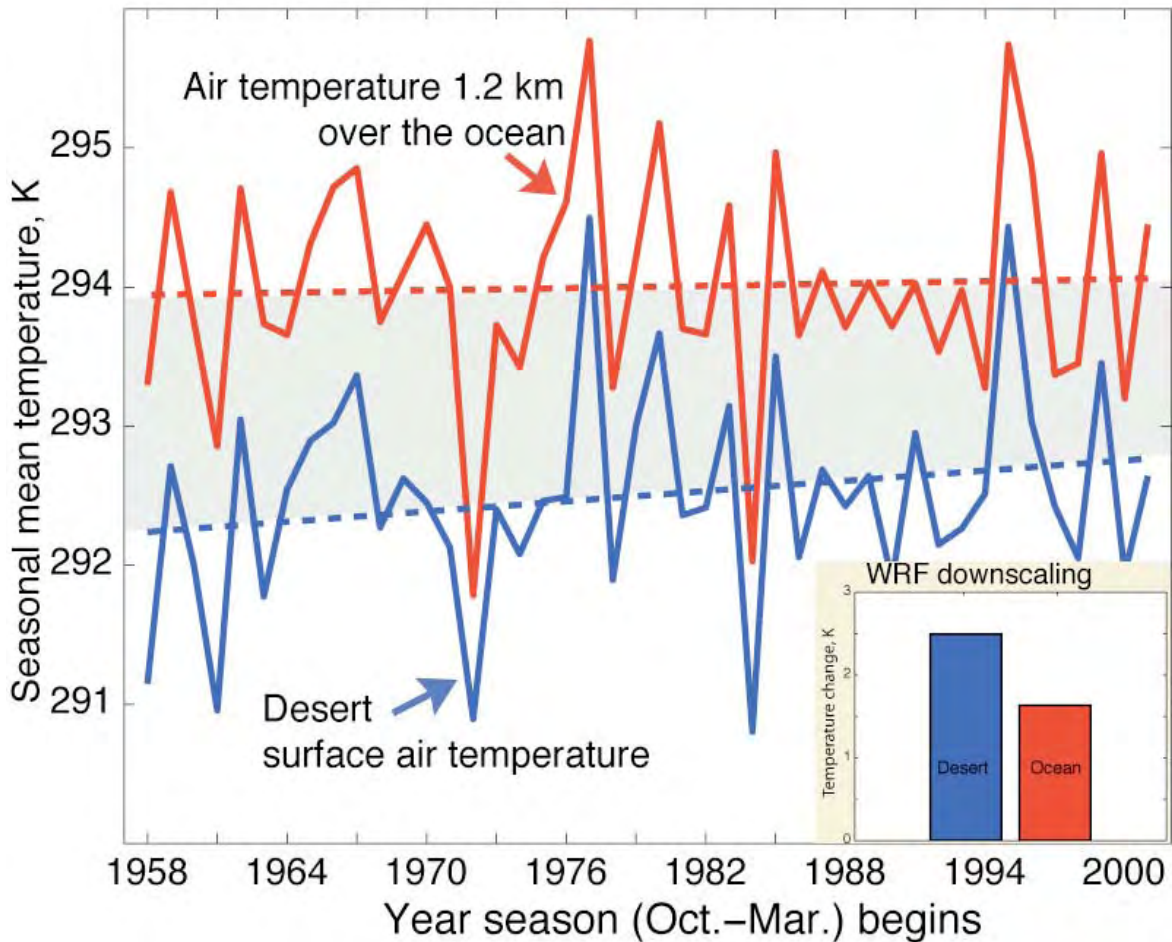


Figure 8. Seasonal mean temperature at the desert surface (blue line) and air temperature 1.2 km above the ocean surface. Dashed lines show linear trend. (Inset) Change in mean temperature between the present and future WRF simulations at the desert surface (blue bar) and 1.2 km over the ocean surface (red bar). Trend in desert surface air temperature is significant at the 90% confidence level using a one-tailed t-test; trend in air temperature over the ocean is not significant.

6.0 Conclusions

This study investigates the frequency of Santa Ana wind events within a high-resolution reconstruction of Southern California’s climate: 44 years (1959–2002) of the ERA-40 reanalysis downscaled to 6-km resolution and two realizations of the NCAR CCSM3 climate, with late-twentieth and mid-twenty-first century greenhouse gas forcing, according to the SRES-A1B emission scenario downscaled to 12-km resolution. The number of Santa Ana days per winter season declines gradually over the 44-year reanalysis period, resulting in over 30% fewer events per year between 1991 and 2001 than between 1959 and 1969. The events per year are similarly reduced in the mid-twenty-first compared with the late-twentieth century, suggesting that the reduction seen in the MM5 downscaling is at least partially caused by a change in the climate due to anthropogenic forcing. This reduction in the frequency of SAs also corresponds with a reduction in their mean intensity.

We use a bivariate regression model to reproduce the Santa Ana time series based on two forcing mechanisms: synoptically-forced strong offshore winds at the mountain tops whose momentum is transported to the surface, and local thermodynamically forced winds caused by a katabatic pressure gradient that arises from the thermal contrast between cold desert air and warmer air over the adjacent ocean. The regression model reproduces approximately 80% of the variability in the Santa Ana time index and also reproduces the dramatic reduction in events in the climate change experiment. We investigate the cause for the reduction of SA frequency using the regression model to partition the forcing into synoptic and katabatic components and find a reduction in katabatic forcing in both simulations. This reduction of katabatic forcing is caused by the larger transient response to increased radiative forcing of desert surface temperature than the air temperature over the ocean at the same altitude. This reduces the likelihood of a large temperature deficit developing in the desert in wintertime and therefore reduces the likelihood of large katabatic forcing.

There are many societal implications of this anthropogenic reduction of Santa Ana wind events that could be significant and should be explored further. The role Santa Ana winds play in spreading wildfire in the region (e.g., Westerling 2004; Keeley 2004) suggests their reduction in frequency could lead to reduced wildfire in Southern California. However, they still occur in the future climate. Moreover, this study does not investigate other critical fire parameters, such as available fuel and relative humidity depression during Santa Anas. Meanwhile, ignition events (i.e., humans lighting matches in the coastal chaparral shrubland), another major factor affecting fire frequency, will probably increase with population (Syphard et al. 2007). This study also has implications for coastal marine ecosystems, which respond favorably to SA conditions, and to the air quality in the Los Angeles basin, which is better during SA events. The ecological effects of nutrient loss for the Southern California Bight and the decline in air quality during winter could be quantified with regional simulations of oceanic biogeochemistry and atmospheric chemistry.

To the extent that the smaller temperature increase in the atmosphere over the ocean is due to the larger oceanic heat capacity, the reduction in thermodynamic forcing of SAs might be a feature of the transient climate change that will return to pre-industrial levels once the climate equilibrates. Nevertheless, the reduction in SA wind events due to anthropogenic climate change is significant because it illustrates an observed and explainable regional change in climate due to plausible mesoscale processes.

7.0 References

- Barry, R. G. 1992. *Mountain Weather and Climate*. London: Routledge. 402 pp.
- Castro, R., A. Mascarenhas, A. Martinez-Diaz-de Leon, R. Durazo, and E. Gil-Silva. 2006. "Spatial influence and oceanic thermal response to Santa Ana events along the Baja California peninsula." *Atmosfera* 19(3): 195–211.
- Chang, S., D. Hahn, C. Yang, D. Norquist, and M. Ek. 1999. "Validation study of the CAPS model and land surface scheme using the 1987 Cabauw/PILPS dataset." *J. Appl. Meteor.* 38:405–422.
- Conil, S., and A. Hall. 2006. "Local regimes of atmospheric variability: A case study of Southern California." *J. Clim.* 19(17): 4308–4325.

- Diffenbaugh, N., J. Pal, R. Trapp, and F. Giorgi. 2005. "Fine-scale processes regulate the response of extreme events to global climate change." *PNAS* 102(44):15 774–15 778.
- Dudhia, J. 1989. "Numerical study of convection observed during the winter monsoon experiment using a mesoscale two-dimensional model." *J. Atmos. Sci.* 46(20): 3077–3107.
- Edinger, J. G., R. A. Helvey, and D. Baumhefner. 1964. Surface wind patterns in the Los Angeles basin during 'Santa Ana' conditions. Part 1 of final rept. on U.S. Forest Service Research Proj. 2606., Univ. of California, Los Angeles, Dept. of Meteorology.
- Finley, J., and M. Raphael. 2007. "The relationship between El Niño and the duration and frequency of the Santa Ana Winds of Southern California." *The Prof. Geog.* 59(2): 184–192. doi:10.1111/j.1467-9272.2007.00606.x.
- Gabersek, S., and D. R. Durran. 2006. "The dynamics of gap flow over idealized topography: Part II. Effects of rotation and surface friction." *J. Atmos. Sci.* 63:2720–2739.
- Grell, G., J. Dudhia, and D. Stauffer. 1994. A description of the fifth-generation Penn State/NCAR Mesoscale Model (MM5). Tech. rep., NCAR Tech. Note NCAR/TN-398+STR.
- Hong, S., and H. Pan. 1996. "Nonlocal boundary layer vertical diffusion in a Medium-Range Forecast Model." *Mon. Wea. Rev.* 124(10): 2322–2339.
- . 1998. "Convective trigger function for a mass flux cumulus parameterization scheme." *Mon. Wea. Rev.* 126:2599–2620.
- Hu, H., and W. Liu. 2003. "Oceanic thermal and biological responses in Santa Ana winds." *Geophys. Res. Lett.* 30(11): 1596. doi:doi:10.1029/2003GL017208.
- Hughes, M., and A. Hall. 2009. The dynamics of the Santa Ana winds. *Clim. Dyn.*, in review.
- Hughes, M., A. Hall, and R. Fovell. 2008. Blocking in areas of complex topography, and its influence on rainfall distribution. *J. Atmos. Sci.* 66(2): 508–518.
- Jickells, T., Z. S. An, K. K. Andersen, A. R. Baker, G. Bergametti, N. Brooks, J. J. Cao, P. W. Boyd, R. A. Duce, K. A. Hunter, H. Kawahata, N. Kubilay, J. laRoche, P. S. Liss, N. Mahowald, J. M. Prospero, A. J. Ridgwell, I. Tegen, and R. Torres. 2005. "Global iron connections between desert dust, ocean biogeochemistry, and climate." *Science* 308:67–71. doi:DOI: 10.1126/science.1105959.
- Kain, J. S. 2002. "The Kain-Fritsch convective parameterization: An update." *J. Appl. Meteor.* 43:170–181.
- Kanamitsu, M., and H. Kanamaru. 2007a. "Fifty-seven-year California reanalysis downscaling at 10 km (CaRD10). Part I: System detail and validation with observations." *J. Climate* 20:5553–5571.
- . 2007b. "Fifty-seven-year California reanalysis downscaling at 10 km (CaRD10). Part II: Comparison with North American Regional Reanalysis." *J. Climate* 20:5572–5592.

- Keeley, J. E. 2004. "Impact of antecedent climate on fire regimes in coastal California." *International J. of Wildland Fire* 13:173–182.
- Leung, L., and S. Ghan. 1999. "Pacific Northwest climate sensitivity simulated by a regional climate model driven by a GCM. Part I: Control simulations." *J. Clim.* 12:2010–2030.
- Miller, N. L., and N. J. Schlegel. 2006. "Climate change projected fire weather sensitivity: California Santa Ana wind occurrence." *Geophys. Res. Lett.* 33. doi:10.1029/2006GL025808.
- Mlawer, E., S. Taubman, P. Brown, M. Iacono, and S. Clough. 1997. "Radiative transfer for inhomogeneous atmosphere: RRTM, a validated correlated-k model for the longwave." *J. Geophys. Res.* 102(D14): 16663–16682.
- Nakicenovic, N., and R. Swart. 2000. *Special Report on Emissions Scenarios*. Edited by Nebojsa Nakicenovic and Robert Swart, pp. 612. ISBN 0521804930. Cambridge, UK: Cambridge University Press, July 2000.
- Parish, T., and J. Cassano. 2003. "Diagnosis of the katabatic wind influence on the wintertime Antarctic surface wind field from numerical simulations." *Mon. Wea. Rev.* 131:1128–1139.
- Raphael, M. N. 2003. "The Santa Ana winds of California." *Earth Interactions* 7:1–13.
- Reynolds, R. W., N. A. Rayner, T. M. Smith, D. C. Stokes, and W. Wang. 2002. "An improved in situ and satellite SST analysis for climate." *J. Climate* 15:1609–1625.
- Schroeder, M. J., M. Glovinsky, D. W. Krueger, V. F. Hendricks, L. P. Mallory, F. C. Hood, A. G. Oertel, M. K. Hull, R. H. Reese, H. L. Jacobson, L. A. Sergius, R. Kirkpatrick, and C. E. Syverson. 1964. *Synoptic weather types associated with critical fire weather*. Tech. rep., Berkeley, Calif., Pacific SW Forest and Range Exp. Sta., Forest Service. U.S. Dept. of Agriculture.
- Skamarock, W., J. Klemp, J. Dudhia, D. Gill, D. Baker, W. Wang, and J. Powers. 2005. A description of the advanced research WRF version 2. Tech. rep., NCAR Tech. Note, NCAR/TN468+STR.
- Smith, T. M., and R. W. Reynolds. 2003. "Extended reconstruction of global Sea Surface Temperatures based on COADS data (1854–1997)." *J. Climate* 16:1495–1510.
- Sommers, W. T. 1978. "LFM forecast variables related to Santa Ana wind occurrences." *Mon. Wea. Rev.* 106:1307–1316.
- Syphard, A., V. Radeloff, J. Keeley, T. Hawbaker, M. Clayton, S. Stewart, and R. Hammer. 2007. "Human influence on California fire regimes." *Ecological Applications* 17:1388–1402.
- Trasvina, A., M. Ortiz-Figueroa, H. Herrera, M. A. Coso, and E. Gonzalez. 2003. "Santa Ana winds and upwelling filaments off northern Baja California." *Dynamics of Atmospheres and Oceans* 37(2): 113–129.

- Trenberth, K., P. Jones, P. Ambenje, R. Bojariu, D. Easterling, A. Klein Tank, D. Parker, F. Rahimzadeh, J. Renwick, M. Rusticucci, B. Soden, and P. Zhai. 2007. Observations: Surface and atmospheric climate change. *Climate Change 2007: The Physical Science Basis. Contribution of Working Group I to the Fourth Assessment Report of the Intergovernmental Panel on Climate Change*. Solomon, S., D. Qin, M. Manning, Z. Chen, M. Marquis, K. Averyt, M. Tignor, and H. Miller, Eds. Cambridge, United Kingdom and New York, NY, USA: Cambridge University Press.
- Uppala, S., P. Kallberg, A. Simmons, U. Andrae, V. da Costa Bechtold, M. Fiorino, J. Gibson, J. Haseler, A. Hernandez, G. Kelly, X. Li, K. Onogi, S. Saarinen, N. Sokka, R. Allan, E. Andersson, K. Arpe, M. Balmaseda, A. Beljaars, L. van de Berg, J. Bidlot, N. Bormann, S. Caires, F. Chevallier, A. Dethof, M. Dragosavac, M. Fisher, M. Fuentes, S. Hagemann, E. Holm, B. Hoskins, L. Isaksen, P. Janssen, R. Jenne, A. McNally, J.-F. Mahfouf, J.-J. Morcrette, N. Rayner, R. Saunders, P. Simon, A. Sterl, K. Trenberth, A. Untch, D. Vasiljevic, P. Viterbo, and J. Woollen. 2005. "The ERA-40 re-analysis." *Quart. J. R. Meteorol. Soc.* 131:2961–3012. doi:doi:10.1256/qj.04.176.
- Westerling, A. L., D. R. Cayan, T. J. Brown, B. L. Hall, and L. G. Riddle. 2004. "Climate, Santa Ana winds and autumn wildfires in Southern California." *EOS* 85(31): 289–296.